NASA

Technical Memorandum 83850

Large-Scale Variations of the Interplanetary Magnetic Field: Voyager 1 and 2 Observations Between 1-5 AU

L.F. Burlaga, R.P. Lepping, K.W. Behannon, L.W. Klein and F.M. Neubauer

OCTOBER 1981

National Aeronautics and Space Administration

Goddard Space Flight Center
Greenbelt, Maryland 20771

NASA

Technical Memorandum 83850

Large-Scale Variations of the Interplanetary Magnetic Field: Voyager 1 and 2 Observations Between 1-5 AU

L.F. Burlaga, R.P. Lepping, K.W. Behannon,
L.W. Klein and F.M. Neubauer

OCTOBER 1981

National Aeronautics and
Space Administration

Goddard Space Flight Center
Greenbelt, Maryland 20771

Large-Scale Variations of the Interplanetary Magnetic Field: Voyager 1 and 2 Observations between 1-5 AU

by

L. F. Burlaga[1)]

R. P. Lepping[1)]

K. W. Behannon[1)]

L. W. Klein[2)]

F. M. Neubauer[3)]

1) NASA/Goddard Space Flight Center
Laboratory for Extraterrestrial Physics
Greenbelt, MD 20771

2) Computer Sciences Corporation
8728 Colesville Road
Silver Spring, MD 20910

3) Institut f. Geophysik der T. U.
Mendelssohnstr. 1
3300 Braunschweig
FEDERAL REPUBLIC OF GERMANY

SUBMITTED TO: Journal of Geophysical Research

ABSTRACT

Observations by the Voyager 1 and 2 spacecraft of the interplanetary magnetic field between 1 and 5 AU have been used to investigate the large-scale structure of the IMF in the years 1977 to 1979, a period of increasing solar activity. This complements the Pioneer 10, 11 investigation between 1-8.5 AU during 1972 to 1976 when the sun was less active. In contrast to the good agreement of the Pioneer observations with the ideal field configuration of the Parker spiral model during near solar minimum conditions, the Voyager spacecraft found notable deviations from that configuration. We attribute these deviations both to temporal variations associated with increasing solar activity, and to the effects of fluctuations of the field in the radial direction. The amplitude of the latter fluctuations were found to be large relative to the magnitude of the radial field component itself beyond approximately 3 AU. The IMF sector structure was generally not well-developed during the period of this study. Notable differences were found between Voyager 1 and Voyager 2 observations. Differences in the region 1-2 AU are attributed to the substantially different latitudes of the two spacecraft during much of the period. Later differences are most likely associated with the fact that the Voyagers moved through the region between 4 and 5 AU at different times. Both Voyager 1 and Voyager 2 observed decreases with increasing heliocentric distance in the amplitude of "transverse" fluctuations in $\underset{\sim}{B}$ which are consistent with the presence of predominantly undamped Alfvén waves in the solar wind, although not necessarily implying the presence of them. The presence of convective structures, compressive modes, and/or a saturated instability of Alfvén waves cannot be excluded by these Voyager results. Fluctuations in the strength of $\underset{\sim}{B}$ (relative to mean field strength) were found to be small in amplitude, with a RMS which is approximately one third of that for the transverse fluctuations, and they are essentially independent of distnce from the sun.

1. Introduction

The large-scale structure of the interplanetary magnetic field (IMF) has been studied extensively both at 1 AU by earth-orbiting spacecraft (Ness and Wilcox 1964, 1967; Burlaga and Ness, 1976; Ness et al., 1971; Fairfield and Ness, 1974; Hedgecock, 1975) and over a wide range of distances from the sun by various deep-space probes. Early observations by Pioneer 6 and Mariners 2, 4 and 5 extended the investigation of the IMF structure to the heliocentric distance range 0.66 to 1.45 AU and also provided data on the radial dependence of the IMF (Burlaga and Ness, 1968; Coleman et al., 1969; Rosenberg and Coleman, 1969, 1973; Villanti and Mariani, 1975). Further studies of the IMF inward to 0.46 and 0.31 AU by Mariner 10 and the Helios spacecraft, respectively (Behannon, 1976a,b; Musmann et al., 1977; Burlaga et al., 1978a,b; Mariani et al., 1978; Neubauer, 1978; Villanti et al., 1979; Behannon et al., 1981), and into the outer solar system to greater than 8 AU by Pioneers 10 and 11 (Smith, 1974, 1979; Rosenberg et al., 1977, 1978; Smith et al., 1978; Thomas and Smith, 1980) have contributed significantly to our understanding of the fundamental global structural characteristics and temporal evolution of the large-scale field (see also review by Behannon, 1978). Pioneer 11, which reached a heliographic latitude of 16°, provided insight into the three-dimensional structure of the field (Rosenberg, 1975; Rosenberg et al., 1977; Smith et al., 1978; see also the review by Smith, 1979).

These and other studies have shown that the large-scale, corotating IMF generally has a structure which is variable in both solar longitude and latitude, with at times a relatively steep gradient present, as a result of the nonuniformity of both the global solar magnetic field and the solar wind. The latter is structured through the presence of bounded, corotating streams originating from discrete source regions on the sun (among numerous studies see Schwenn et al., 1978; Mitchell et al., 1981; and the review by Hundhausen, 1979). This structure is subsequently modified through interactions between fast and slow streams (Hundhausen, 1972, Burlaga, 1974; Gosling et al., 1978; Rosenberg and Coleman, 1980). Pioneers 10 and 11 have demonstrated the continued evolution of stream profiles and interaction region signatures to distances beyond 5 AU (Smith and Wolfe,

1976, 1977). In addition to thse stream effects, the magnetic field polarity sectoring observed in and near the ecliptic plane has been found to depend on the location of the neutral surface at the photosphere and to vary over the solar cycle (Burlaga et al., 1978a; Klein and Burlaga, 1980; Hundhausen, 1979; Svalgaard and Wilcox, 1978; and others).

In a very gross sense, the average IMF is consistent with the Parker formulation for a uniform, Archimedean spiral field (Parker, 1958). According to this model (hereafter called the "spiral model") power law radial distance dependences for the radial and azimuthal field components are predicted to have exponents of -2 and -1, respectively, and $B_\theta \equiv 0$. This model most nearly holds for long-term averages of the measured field. There is considerable variability on time scales shorter than a solar rotation as a result of the long-term, temporal evolution of the source field at the sun and the stream source regions (King, 1979, 1981; Barouch and King, 1975; Burlaga and King, 1979). Both the short-term and the long-term variability increase as solar activity increases. The purpose of this present study is to investigate the large-scale structure of the IMF in the region between 1 AU and $\gtrsim$ 5 AU, in the years 1977 to 1979 using Voyager 1 and 2 data. This complements the Pioneer 10, 11 investigation of the large-scale structure between 1-8.5 AU in the years 1972 to 1976, when the sun was less active.

The Voyager 1 and 2 spacecraft were launched on September 5, 1977 and August 20, 1977, respectively, and arrived at Jupiter at $\gtrsim$ 5 AU on March 5 (Voyager 1) and July 9, 1979 (Voyager 2). The Voyager dual fluxgate magnetometer systems have been described in detail by Behannon et al., (1977). The period of cruise to Jupiter was at a time of increasing solar activity, compared with the near solar minimum conditions that prevailed during the earlier Pioneer studies. We shall show that notable deviations from the ideal spiral configuration were observed by the Voyager spacecraft at this time. We attribute these deviations both to temporal variations associated with the increase in solar activity, and to the effects of fluctuations of the field in the radial direction. The amplitude of these fluctuations is found to be large relative to the magnitude of the radial field component itself at distances beyond $\sim$ 3 AU.

2. Radial Variation of the Magnitude and Direction of B

One can examine the radial variations of $\underset{\sim}{B}$ in at least three different ways, each of which provides unique and valuable insights. First, one can simply plot the magnitude of $\underset{\sim}{B}$, $|\underset{\sim}{B}| \equiv B$, and two angles (λ, δ) as functions of R. We use heliographic equatorial coordinates, in which $\hat{R}$ points away from the sun, $\hat{T}$ is parallel to the solar equatorial plane and in the direction of motion of the planets, and $\hat{N}$ forms a right-handed system. The angle δ is the elevation of $\underset{\sim}{B}$ with respect to the $\hat{R}$-$\hat{T}$ plane, and λ is the azimuth, being zero for $\underset{\sim}{B}$ radially outward and increasing counterclockwise when viewed from the north. Second, one can plot distributions of the differences between the observed and predicted values of $B(R) - B_P(R)$, $\lambda(R) - \lambda_P(R)$ and $\delta(R) - \delta_P(R)$ for successive distance intervals, which we take in increments of 1 AU. Third, one can plot components of $\underset{\sim}{B}$ as a function of R, viz., $\underset{\sim}{B} = B_R \hat{R} + B_T \hat{T} + B_N \hat{N}$. We shall consider each of the above approaches in turn. Our aim is to assess the validity of the spiral model as a lowest order description of the interplanetary magnetic field, and to examine the departures from this model both as a function of distance and of time.

We consider 24-hour averages of the magnetic field throughout this paper. The 24-hour average of the magnetic field strength, B, is computed from hour-averages of the magnitude of $\underset{\sim}{B}$, and the corresponding angles (λ, δ) are computed from hour averages of the components $\underset{\sim}{B}$ ($< B_R > = B \cos\delta \cos\lambda$, $< B_T > = B \cos\delta \sin\lambda$, $< B_N > = B \sin\delta$).

The radial variation of B measured by Voyager 1 is shown in Figure 1. Note that B is plotted on a log scale, which tends to reduce the enhancements in B and enhance the depressions in B. This format has the advantage that the relative changes in B may be compared directly at all distances. For example, if B_{max}/B_{min} were the same for stream-related perturbations at all distances, then $\log B_{max} - \log B_{min}$ would be a constant, and the scatter from the spiral model would be the same at all distances. On a linear scale, changes in B at large distances, where B is small, would be difficult to see and evaluate, but this problem does not occur on a log

scale. The curve in Figure 1 is the best fit of the theoretical curve $B_p = (A/R^2)(R^2 + 1)^{1/2}$ to the data on a semi-log scale where R is in AU; we assume that $(\Omega R_1/V) = 1$ (Ω is the angular speed of the sun, R_1 is 1 AU, and V is the solar wind speed). For Voyager 1, A = 4.5 nT (corresponding to mean value for B of 6.4 nT at 1 AU). This curve provides a reasonably accurate description of the overall decrease of B with R, but the fluctuations about the curve are often large. The fluctuations are real and too large to attribute to changes in Ω/V alone. It will be shown in subsequent papers that they are associated with specific flow systems and dynamical processes which cannot be accounted for by the stationary spiral model. Thus, while the spiral model provides a zeroth order description of the observed B(R), the predicted field strength at a given distance/time is often in error by a factor of two or more.

The direction of $\underset{\sim}{B}$ observed by Voyager 1 (see Figure 1) fluctuates about the solar equatorial plane, $\delta = 0$, as expected from the spiral model, but again the fluctuations can be large at times. More interesting is the longitudinal angle, $\lambda(R)$. Since the polarity of the field can be either positive ($\underset{\sim}{B}$ pointing away from the sun) or negative ($\underset{\sim}{B}$ pointing toward the sun), the spiral model gives two curves for $\lambda(R)$ as shown in Figure 1, computed from $\lambda_p = -\tan^{-1}R$ assuming that $\Omega R_1/V = 1$. At 1 AU, for example, λ_p can be either 135° or 315° for $\Omega R_1/V = 1$. Although the data show some tendency to follow the theoretical curves, there is considerable scatter, and the sector structure is not well-defined. Departure from the spiral model curves is large even near 1 AU where it is known from previous studies that the spiral model often provides a good description of the data, and the data actually are closer to the theoretical curves at larger distances. Thus, we attribute the departure of the data from the spiral model curves to temporal variations. The solar wind was unusually disturbed during the months following the launches of Voyagers 1 and 2, corresponding to the increase in solar activity associated with the new solar cycle. We stress again that Parker's spiral model is a stationary model which cannot describe dynamical processes.

The Voyager 2 results for B(R), $\delta(R)$, and $\lambda(R)$ are shown in Figure 2. In general, they are similar to the Voyager 1 results. The best fit curve

to B(R) gave A = 4.0, which is somewhat lower than the Voyager 1 value but not inconsistent with it. Again the fluctuations in B are large, the direction of $\underset{\sim}{B}$ fluctuates about the equatorial plane, the field is often far from the nominal spiral direction, and the sector structure is generally not well-developed.

3. Distributions of B, λ and δ as a Function of Distance

We have seen that the magnetic field fluctuates considerably about the spiral model, and in this section we shall show the actual distributions of B, δ and λ. Again we work with 24-hour averages, and in order to have good statistics, we consider data in increments of 1 AU, corresponding to time intervals ranging from ∿ 100 to ∿ 200 days. The fluctuations about the spiral model are shown most clearly by subtracting the theoretical values from each daily average, i.e., we computed the distributions of log B(R) - log B_p(R) = log (B/B_p), δ(R) = 0, and λ(R) - λ_p(R) for data between 1-2 AU, 2-3 AU, 3-4 AU and 4-5 AU. The results are shown in Figures 3-6 for the Voyager 1 and 2 data.

In FIgure 3, we show the distribution of log B/B_p rather than B because 1) it is consistent with the results in Figures 1 and 2, 2) it allows us to compare the distributions at all distances in a meaningful way, and 3) other authors (e.g., Burlaga and King, 1979) have shown that a distribution of log B is more nearly gaussian than the distribution of B, which is highly skewed by a tail at large B. The distribution peaks close to the spiral model value, B/B_p = 1, but it is skewed in favor of lower values. At larger distances (later times) both the mode and the median are at B/B_p > 1, i.e., the fields are stronger than predicted by the fit to the spiral model. The Voyager data alone do not allow us to determine whether this is a radial variation or a temporal variation (the measurements near 5 AU were made more than a year after those near 1 AU). To distinguish among temporal and spatial variations, we consider the distributions of B obtained at 1 AU by IMP spacecraft in the years 1976, 1977, 1978 and 1979, shown in Figure 4. It is apparent that the field strength was increasing during this period, and the change was due to a general displacement of the histogram rather than simply an effect due to a skewing of the

distribution. King (1981) has reported that the mean field strength increased from 5.4 nT in 1977 to 6.7 nT in 1979. This increase, which presumably reflects an increase in the solar magnetic field strength, is sufficient to account for the trends in the Voyager 2 data seen in Figure 3. It is possible that better agreement between the observations and the spiral model could be obtained by allowing A to vary slowly with time in the expression $B = (A(t)/R^2)\ (R^2 + 1)^{1/2}$.

Comparing the Voyager 2 data with the Voyager 1 data for the distributions of log (B/B_p) (see Figure 3), one sees differences that cannot be explained solely by an increase in the mean field, although that effect can also be seen between launch and day August 25, 1978. The greatest difference between Voyager 1 and 2 results is in the histogram for 4-5 AU, the Voyager 1 histogram being broader and having a median closer to $B/B_p = 1$. The difference is probably due to the fact that the two spacecraft sampled the region 4-5 AU at different times; Voyager 2 reached 4 AU 40 days after Voyager 1 and it reached 5 AU $\sim$ 100 days later than Voyager 1. The differences between the histograms at distances less than 4 AU are smaller, as expected, because the two spacecraft passed through each region in more nearly the same time interval.

The distributions in Figure 3 are not smooth and there are differences in detail between the Voyager 1 and 2 results partly because of the limited statistics. There are approximately 100 to 200 points in each of the histograms, so the uncertainty in the peak values, which are near a fractional value F = 0.1, are approximately $(0.1 \times 100)^{1/2}/100$ to $(0.1 \times 200)^{1/2}/200$ or $\sim$ 0.02 to 0.03; similarly, the corresponding uncertainties at F = 0.05 are $\sim$ 0.015 to 0.02.

Now consider the behavior of the azimuthal direction of the magnetic field shown by the distributions of $\lambda - \lambda_p$ in Figure 5. In this case we used the measured speeds and calculated the theoretical value $\lambda_p = \tan^{-1}((\Omega R_1/V\ R)$, R in AU, whenever measurements of V were available; for times when measurements of V were not available, we set V = 400 km/s. The spiral model predicts two peaks, one at $\lambda - \lambda_p = 0$, and another at $\lambda - \lambda_p = 180°$. Figure 5 shows a general tendency for peaks to occur at the theoretical

values, but the peaks are broad, and often the field direction is perpendicular to the spiral direction near $\lambda \sim \lambda_p \approx 90°$. Thus, while the spiral model gives a useful zeroth order description, the field is often far from the nominal directions and the fluctuations about the spiral direction cannot be disregarded. Comparing Voyager 1 and 2 results, one sees that there are large differences at all distances. Although the statistical errors are larger here than in Figure 3 because the data are spread out into more "bins", they cannot account for the major differences that are observed. Between 4-5 AU where the greatest differences occur, Voyager 2 observed fields close to the spiral direction and primarily of negative polarity, whereas Voyager 1 observed a rather broad distribution with more nearly equal positive and negative polarities. The latitudinal separation was $\lesssim 0.9°$, so it is unlikely that the difference is simply a spatial effect related to the position of the current sheet. The difference is probably a temporal effect, since the two spacecraft moved between 4-5 AU at very different times--a few solar rotations apart. The differences between the histograms for 3-4 AU and 2-3 AU being smaller is consistent with the smaller difference in times corresponding to the transits by Voyager 1 and 2. However, the histogram differences for 1-2 AU are surprisingly large, considering that the two spacecraft moved through this region in nearly the same time interval (November 18, 1977 to January 10, 1978 for Voyager 2 and September 5, 1977 to January 9, 1978 for Voyager 1). This difference may be related to the fact that the two spacecraft were at substantially different latitudes (the latitude difference became as large as 3.7°) during much of this period, for it is known that sector structure can be very sensitive to spacecraft latitude (Smith, 1979; Villante et al., 1979 Burlaga et al., 1981).

Finally, consider the distributions of δ angles for Voyager 1 and 2 as a function of distance, shown in Figure 6. The most probable value is within 10° (the bin size) of the spiral model value in every case. There are some differences in the shape of the distributions, especially at 4-5 AU and to a lesser extend at 3-4 AU, which can be attributed to temporal variations, and there are differences in detail owing to the statistical uncertainties. In general, however, the spiral model provides a rather satisfactory description of the δ-angle of the field. This of course

follows from the assumption that $\delta = 0°$ near the solar equator, which is motivated by symmetry considerations.

4. Radial Variations of the Cartesian Components of B

The equations for the spiral field model are simplest when the components of $\underset{\sim}{B}$ are described in an orthonormal/spherical coordinate system: $\pm B_R \propto r^{-2}$, $\pm B_T \propto r^{-1}$, $B_N = 0$. In practice it is necessary to plot average values for those components (we use 24-hr averages), and for this some care is required because of the presence of sector boundaries and fluctuations. Suppose, for example, that there is a sector boundary in the middle of the averaging interval. Then B_R and B_T are positive in one half of the interval and negative in the second half, giving $\langle B_R \rangle = \langle B_T \rangle = 0$ even if the field strength is constant and non-zero throughout the interval. This artifact can be removed by computing $\langle |B_R| \rangle$ and $\langle |B_T| \rangle$. However, when one takes the average of an absolute magnitude the fluctuations do not "average out". For example, we have seen in Figures 1, 2 and 6 that δ fluctuates about zero, which means that B_N fluctuates about zero. In this case one might have $\langle B_N \rangle = 0$ but $\langle |B_N| \rangle \neq 0$. Similarly, if $B_R = B_{RP} + \Delta B$ and if $\Delta B \gtrsim B_{RP}$, where B_{RP} is the nominal spiral model value and ΔB is a fluctuations component, then $\langle |B_R| \rangle > \langle B_R \rangle$. This must be considered in dealing with real data, in which dynamical fluctuations are always present, and one should note that the spiral model assumes that no fluctuations are present, i.e., that $\Delta B = 0$. A third method, which avoids the difficulties of those two approaches, is to use sector-weighted averages, which means that one must decide in advance which polarity is appropriate (e.g., Rosenberg et al., 1978). The problem with this approach is that one must introduce an arbitrary criterion for identifying positive and negative polarities, and this can be a serious ambiguity when the field is far from the spiral direction, as it frequently is for the data set under consideration (see Figures 1 and 2). We shall present results obtained using only the first two methods: 24-hour averages of the magitudes of B_R, B_T, B_N; and magnitudes of 24-hour averages of these quantities.

Figure 7 shows the Voyager 1 observations of $< B >$, $< |B_R| >$, $< |B_T| >$ and $< |B_N| >$ as functions of distance between 1-5 AU, on a log-log scale. The panel showing $< B >$ vs. R gives the same data as Figure 1 in a slightly different format. The corresponding curve is the best fit described in Section 2, and again one sees that it gives a satisfactory zeroth order approximation but does not account for the rather large fluctuations on a smaller scale.

The data for $< |B_R| >$ vs R in Figure 7 give results which are unexpected and inconsistent with the spiral model. Near 1 AU the data scatter about a value which is close to the average value measured at 1 AU (King, 1981), and close to that given by the linear least squares fit to the data, but near 5 AU the data lie primarily above the spiral model. The discrepancy is seen also in the exponent obtained from the least squares fit, viz. $< |B_R| > \propto R^{-1.56 \pm 0.06}$ which is to be compared with R^{-2} predicted by the spiral model. The inability of the spiral model to fit the data can be attributed to its neglect of the effect of fluctuations. The effect of such fluctuations on the fits can be estimated as follows. It was shown above that the field direction fluctuates about $\delta = 0°$, hence $< |B_N| >$ represents the effects of fluctuations. A least squares fit to $< |B_N| >$ vs R (see Figure 7) gives $1.9\ R^{-1.18}$, so that $< |B_N| >$ exceeds the predictions of the spiral model beyond 2.5 AU. This is illustrated by the lines in Figure 7, where one sees that the spiral model line for $B_R(R)$ intersects the best fit curve for $< |B_N| >$ vs R (which represents the fluctuations) at $\sim$ 2.5 AU. Near 1 AU $< |B_R| >$ is primarily a measure of the large-scale field, but near 5 AU it is primarily a measure of the fluctuations. In other words, the radial component of the large-scale field given by the spiral model is in the "noise" beyond $\sim$ 2.5 AU.

At large distances from the sun, the principal component of the field is B_T, since this falls off more slowly than $B_R(R)$. Figure 7 shows the observations of $< |B_T| >$ versus R for the Voyager 1 data, together with the linear least squares fit, $< |B_T| > (R) = 3.3\ R^{-1.2}$. This is everywhere larger than the fluctuation level represented by $< |B_N| >$. It falls off somewhat more rapidly with R than predicted by the spiral model ($R^{-1.2}$ instead of R^{-1}), but the uncertainty on the exponent is $\pm$ 0.7 and the

scatter of the points about the best-fit line is large, so the discrepancy is not very significant.

The corresponding results for $< |B| >$, $< |B_T| >$ $< |B_R| >$, and $< |B_N| >$ versus R for the Voyager 2 data are summarized by the parameters describing the least squares fits, listed in Table 1. The radial variation of $< |B_R| >$ is essentially the same for Voyager 1 and 2, viz. $R^{-1.56 \pm 0.06}$ and $R^{-1.47 \pm 0.05}$, respectively. The fits to $< |B_T| >$ versus R give a decline for Voyager 1 data which is more rapid than predicted by the spiral model ($R^{-1.20 \pm 0.07}$) whereas they give a decline for Voyager 2 data which is less rapid than predicted ($R^{-0.80 \pm 0.06}$). It is possible that this is just a statistical effect, but recall that Voyager 1 and 2 sampled the outer regions at different times, and near 1 AU they were at different latitudes, so we should not expect them to measure exactly the same results. The fits to $< |B_N| >$ versus R and $< B >$ versus R give the same exponents, within the uncertainties, for Voyager 1 and 2.

The scatter plots for the magnitudes of the 24-hr averages--$|< B_T >|$, $|< B_R >|$ and $|< B_N >|$--versus R are shown in Figure 8 for the Voyager 1 data. Here one sees much more scatter than in Figure 7 mostly due to the appearance of low values. This is expected since sector boundaries, filaments and fluctuations can give averages which are small or even zero. For example, the length of the interval in question is $\sim$ 500 days (18 solar rotations) for Voyager 1 and $\sim$ 600 days (22.5 solar rotations) for Voyager 2; assuming 4 sector boundaries per solar rotation, one expects 75 to 90 "low" points from this effect alone. Because of the presence of artifically low values, the intercepts of the least-squares-fit lines in Figure 8 are smaller than those in Figures 7 (see Table 1). However, the exponents describing the radial variations are not very sensitive to the averaging method used. In particular, one finds for Voyager 1 that:

$< |B_R| > \sim R^{-1.56 \pm 0.06}$ versus $|< B_R >| \sim R^{-1.57 \pm 0.11}$; $< |B_T| > \sim R^{-1.20 \pm 0.07}$ versus $|< B_T >| \sim R^{-0.92 \pm 0.010}$; and $< |B_N| > \sim R^{-1.18 \pm 0.07}$ versus $|< B_N >| \sim R^{-0.92 \pm 0.12}$.

We shall not show the corresponding scatter plots for the Voyager 2 data, but they closely resemble Figure 8. The best fit results are given in Table 1, where one sees that they are insensitive to the averaging method used, and the Voyager 2 results are similar to the Voyager 1 results. The only exception to this last remark is the behavior of the B_T component whose exponent is larger for Voyager 2 than for Voyager 1. Note that even though B_T is the principal contributor to $\underset{\sim}{B}$, and B_T is different for Voyagers 1 and 2, the radial variation of B is essentially the same for both spacecraft, viz. $R^{-0.15 \pm 0.12}$ for Voyager 1 and $R^{-0.14 \pm 0.11}$ for Voyager 2.

Summarizing the results of this section, we find that: 1) $B_R(R)$ appears to fall off less rapidly than predicted by the spiral model, probably because the nominal value is smaller than the level of fluctuations beyond $\sim$ 2.5 AU, 2) The exponent describing the radial variation of $B_T(R)$ varies from -0.56 to -1.20, depending on the data and the averaging method used; 3) The amplitude of the normal component B_N is non-zero even when one considers $|< B_N >|$, and the exponent describing its radial variation is approximately -1.05 ± 0.1.

5. Radial Variations of the Fluctuations in $\underset{\sim}{B}$

We have seen that the fluctuations in $\underset{\sim}{B}$ with respect to the spiral model can be large even when 24-hr averages are used. In this section we shall consider the variances on a smaller scale--those associated with the individual hour averages. These represent the microscale structure of the solar wind, and they carry information about Alfvénic fluctuations, discontinuities, etc., that occur on a scale $\lesssim$ 0.01 AU. For each hour, there are two variances of interest: $\sigma_B^2 = N^{-1} \sum_i (B_i - < B >)^2$, where B_i is the field strength measured with a resolution of 48 sec and $< B >$ is the average field strength during the hour; and

$$\sigma_c^2 = N^{-1} \sum_i [(X_{Ri} - < X_R >)^2 + (X_{Ti} - < X_T >)^2 + (X_{Ni} - < X_N >)^2],$$

where X_{Ri}, etc., are the components of $\underset{\sim}{B}$. We shall consider 24-hour averages of σ_c, σ_c/B and σ_B/B.

The quantity $< \sigma_c >$ versus R, to which transverse fluctuations in $\underset{\sim}{B}$ are the dominant contributor, is shown in Figure 9 for both Voyager 1 and 2. This clearly decreases with distance from the sun, and linear least squares fits give $\sigma_c \sim R^{-1.52 \pm 0.07}$ and $R^{-1.33 \pm 0.06}$ for Voyager 1 and 2, respectively (see Table 1). These results are consistent with one another, and they are consistent with an $R^{-3/2}$ law, which is the prediction for Alfvén waves propagating outward without attenuation in a spherically symmetric solar wind (Whang, 1973; Hollweg, 1974; Belcher and Burchsted, 1974). Similar results have been found in data from previous experiments at different distances and times. Although consistent with predominantly undamped Alfvén waves, it does not necessarily imply the presence of them. In particular, we cannot exclude the presence of convective structures and compressive modes, and we cannot exclude a saturated instability of Alfvén waves. This last point is clear from Figure 10, which shows that $< \sigma_c/B >$ is nearly constant at ~ 0.3 varying only as $R^{-0.23 \pm 0.05}$ and $R^{-0.32 \pm 0.05}$ for Voyager 1 and 2, respectively. Thus, the value of $< \sigma_c/B > \sim 0.3$ could be a saturation effect (Mariani et al., 1978).

Finally, let us consider the fluctuations in the strength of $\underset{\sim}{B}$ relative to this mean field strength. Figure 11 shows $< \sigma_B/B >$ 24-hr versus R for Voyagers 1 and 2. The least squares fits show that this is essentially independent of distance with a value of approximately 0.09 ± 0.07, averaging over Voyager 1 and 2 (see Table 1). Thus, the variations in B are small, with an RMS which is approximately one third of that for the transverse fluctuations. This is again consistent with earlier results (see Behannon, 1978). Although small, they are nevertheless real and significantly above the limits of sensitivity of the instrument (quantization uncertainty ± 0.0022 nT) or the typical sensor noise level (0.006 nT RMS over 8.3 Hz).

Summary

We have described and discussed the large-scale structure of the

the spiral field model gives a reasonable zeroth order description, but at any given time the measured daily average of $|\underset{\sim}{B}|$ or a component of $\underset{\sim}{B}$ may differ from the predicted value by a factor of 2 or more. The variability observed by Voyagers 1 and 2 is apparently significantly greater than that observed in the same region by Pioneers 10 and 11 from 1972 to 1975. The difference is probably related to the fact that Voyagers 1 and 2 passed through the region at a time of increasing solar activity when there were many transient disturbances, whereas Pioneer 10 and 11 passed through the region in the declining phase of the solar cycle when the solar wind was highly ordered and changed relatively slowly. The effect of temporal variations was observed directly by Voyagers 1 and 2 themselves, between 4 and 5 AU, for they observed appreciably different magnetic field distributions ($|\underset{\sim}{B}|$, λ, and δ) in this region even though they followed nearly the same trajectory. We attribute this to temporal variations of the interplanetary medium, because Voyager 2 traversed the region $\sim$ 50 days later than Voyager 1.

It is customary to plot the B_R, B_T and B_N components of $\underset{\sim}{B}$ versus R since the theoretical expression for these variations is a simple power law. We found that the radial (B_R) component falls off more slowly with R than is predicted. We attribute this to the effect of a spectrum of fluctuations, which is always present but is ignored in the spiral model. We estimate that beyond $\sim$ 2.5 AU the fluctuations in the radial direction (e.g., due in part to transverse fluctuations in $\underset{\sim}{B}$) are larger than the theoretical B_R component, which falls off rather fast with R (R^{-2}). The azimuthal component of $\underset{\sim}{B}$ (B_T) falls off less rapidly with distance than the radial component and it remains larger than the fluctuations in the field out to 5 AU. Correspondingly, the observed variation of B_T with R is in better agreement with the spiral model than the radial component.

If the solar wind is changing while a spacecraft moves from 1 to 10 AU a simple least square fit to B_R and B_T need not have an R^{-2} and R^{-1} dependence respectively, even if there are no fluctuations present. The spiral model is a stationary model, and the solutions may be different for different times: $B_R = B_{Ro}(t)\ R^{-2}$, $B_T = B_{To}(t)\ R^{-1}$. Accordingly, data obtained over a long time interval could give "anomalous" radial

dependences for B_R and B_T if the source conditions change during the interval. We have shown (Figure 4) that the mean field strength increased between 1977 and 1979. If this were due entirely to a change in the B_R component, one would expect to observe $B_R \propto R^{-1.9}$ instead of R^{-2}. In fact, we observe $B_R \propto R^{-1.5}$, so the long term variation cannot account for this dependence. As discussed above, the $R^{-1.5}$ dependence is more likely to be the result of the fluctuations that are present.

We have also considered the radial variation of the 24-hr averages of the hour-average RMS σ_c (due to small-scale fluctuations in all the components of $\underset{\sim}{B}$) and of σ_B/B (due to small-scale fluctuations in the magnitude of $\underset{\sim}{B}$. We found that the variation of $\sigma_c(R)$ was consistent with the prediction of Alfvén waves propagating outward without attenuation, but we also noted that σ_c/B was approximately constant, consistent with a saturation effect. In general, $\sigma_B \neq 0$, so the fluctuations are not pure Alfvén waves, and one expects contributions due to small-scale inhomogeneities and large-scale gradients in B. Nevertheless, $\sigma_B << \sigma_c$, and the fluctuations are Alfvénic in this sense.

Acknowledgments

We thank the principal investigator of the magnetic field experiment, N. F. Ness, and co-investigator and principal engineer, M. Acuna, for their support of this work. We also wholeheartedly thank all those concerned with the considerable Voyager data processing effort, including W. H. Mish, D. R. Howell, A. D. Silver, G. M. Burgess, T. P. Carleton, L. J. Moriarty, M. J. Silverstein, P. Harrison, M. Schmitz and T. Vollmer.

REFERENCES

Barouch, E., and J. H. King, A survey of the interplanetary magnetic field, Int. Cosmic Ray Conf. 14th, 3, 1036, 1975.

Behannon, K. W., Observations of the interplanetary magnetic field between 0.46 and 1 AU, by the Mariner 10 spacecraft, Ph. D. thesis, Catholic Univ. of America, Washington, D. C., 1976a. (Also NASA/GSFC X Doc. 692-76-2, Jan. 1976).

Behannon, K. W., Mariner 10 interplanetary magnetic field results, in Physics of Solar Planetary Environments, vl. 1, edited by D. J. Williams, p. 332, AGU, Washington, D. C., 1976b.

Behannon, K. W., Heliocentric distance dependence of the interplanetary magnetic field, Rev. Geophys. Space Phys., 16, 125, 1978.

Behannon, K. W., M. H. Acuna, L. F. Burlaga, R. P. Lepping, N. F. Ness, and F. M. Neubauer, Magnetic field experiment for Voyagers 1 and 2, Space Sci. Rev., 21, 235, 1977.

Behannon, K. W., F. M. Neubauer, and H. Barnstorf, Fine-scale characteristics of interplanetary sector boundaries, J. Geophys. Res., in press, 1981.

Belcher, J. W., and R. Burchsted, Energy densities of Alfvén waves between 0.7 and 1.6 AU, J. Geophys. Res., 79, 4765, 1974.

Burlaga, L. F., Interplanetary stream interfaces, J. Geophys. Res., 79, 3717, 1974.

Burlaga, L. F., and J. H. King, Intense interplanetary magnetic fields observed by geocentric spacecraft during 1963-1975, J. Geophys. Res., 84, 6633, 1979.

Burlaga, L. F. and N. F. Ness, Macro- and micro-structure of the interplanetary magnetic fields, Can. J. Phys., 46, 5962, 1968.

Burlaga, L. F. and N. F. Ness, The large scale magnetic field in the solar wind, in Proceedings of the Symposium on the Study of the Sun and Interplanetary Medium in Three Dimensions, NASA/GSFC X Doc. 660-76-53, edited by L. A. Fisk and W. I. Axford, p. 142, NASA/Goddard Space Flight Center, Greenbelt, Md., 1976.

Burlaga, L. F., K. W. Behannon, S. F. Hansen, G. W. Pneuman, and W. C. Feldman, Sources of magnetic fields in recurrent interplanetary streams, J. Geophys. Res., 83, 41771, 1978a.

Burlaga, L. F., N. F. Ness, F. Mariani, B. Bavassano, U. Villante, H. Rosenbauer, R. Schwenn, and J. Harvey, Magnetic fields and flows between 1 and 0.3 AU during the primary mission of Helios 1, J. Geophys. Res., 83, 5167, 1978b.

Burlaga, L. F., A. J. Hundhausen and Zhao Xue-Pu, The coronal and interplanetary current sheet in early 1976, J. Geophys. Res., in press, 1981.

Coleman, P. J., Jr., E. J. Smith, Davis, L., Jr., and D. E. Jones, The radial dependence of the interplanetary magnetic field: 1.0-1.5 AU, J. Geophys. Res., 74, 2826, 1969.

Fairfield, D. H. and N. F. Ness, Interplanetary sector structure: 1970-1972, J. Geophys. Res., 79, 5089, 1974.

Gosling, J. T., J. R. Asbridge, S. J. Bame, and W. C. Feldman, Solar wind stream interfaces, J. Geophys. Res., 83, 1401, 1978.

Hedgecock, P. C., The heliographic latitude dependence and sector structure of the interplanetary magnetic field 1969-1974: Results from the HEOS satellites, Solar Phys., 44, 205, 1975.

Hollweg, J. V., Transverse Alfvén waves in the solar wind, J. Geophys. Res., 79, 1539, 1974.

Hundhausen, A. J., Coronal Expansion and Solar Wind, Vol. 5, Physics and Chemistry in Space, Springer-Verlag, New York, 1972.

Hundhausen, A. J., Solar activity and the solar wind, Rev. Geophys. Space Phys., 17, 2034, 1979.

King, J. H., Solar cycle variations in IMF intensity, J. Geophys. Res., 84, 5938, 1979.

King, J. H., On the enhancement of the IMF magnitude during 1978-1979, J. Geophys. Res., 86, 4828, 1981.

Klein, L., and L. F. Burlaga, Interplanetary sector boundaries 1971-1973, J. Geophys. Res., 85, 2269, 1980.

Mariani, F., N. F. Ness, L. F. Burlaga, B. Bavassano, and U. Villante, The large-scale structure of the interplanetary magnetic field between 1 and 0.3 AU during the primary mission of Helios 1, J. Geophys. Res., 83, 5161, 1978.

Mitchell, D. G., E. C. Roelof, and J. H. Wolfe, Latitude dependence of solar wind velocity observed at $\geq$ 1 AU, J. Geophys. Res., 86, 165, 1981.

Musmann, G., F. M. Neubauer, and E. Lammers, Radial variation of the interplanetary magnetic field between 0.3 AU and 1.0 AU; Observations by the Helios-1 spacecraft, Z. Geophys., 42, 591, 1977.

Ness, N. F. and J. M. Wilcox, Solar origin of the interplanetary magnetic field, Phys. Rev. Lett., 13, 461, 1964.

Ness, N. F. and J. M. Wilcox, Interplanetary sector structure, 1962-1966, Solar Phys., 2, 351, 1967.

Ness, N. F., A. J. Hundhausen, and S. J. Bame, Observations of the interplanetary medium, Vela 3 and IMP 3, 1965-1967, J. Geophys. Res., 76, 6643, 1971.

Neubauer, F. M., Recent results on the sector structure of the interplanetary magnetic field, in Proceedings of the Second European Solar Meeting "Highlights of Solar Physics", Toulouse, France, March 8-10, 1978.

Parker, E. N., Dynamics of the interplanetary gas and magnetic fields, Astrophys. J., 128, 664, 1958.

Rosenberg, R. L., Heliographic latitude dependence of the IMF dominant polarity in 1972-1973 using Pioneer 10 data, J. Geophys. Res., 80, 1339, 1975.

Rosenberg, R. L. and P. J. Coleman, Jr., Heliographic latitude dependence of the dominant polarity of the interplanetary magnetic field, J. Geophys. Res., 74, 5611, 1969.

Rosenberg, R. L. and P. J. Coleman, Jr., The radial dependence of the interplanetary magnetic field: 1.0-0.7 AU, Inst. Geophys. and Planet. Phys. Publ. No. 1196-26, U. of California, Los Angeles, 1973.

Rosenberg, R. L. and P. J. Coleman, Jr., Solar cycle-dependent north-south field configurations observed in solar wind interaction regions, J. Geophys. Res., 85, 3021, 1980.

Rosenberg, R. L., M. G. Kivelson, and P. J. Coleman, Jr., The radial dependence of the interplanetary magnetic field between 1 and 5 AU: Pioneer 10, J. Geophys. Res., 83, 4165, 1978.

Rosenberg, R. L., M. G. Kivelson, and P. C. Hedgecock, Heliographic latitude dependence of the dominant polarity of the interplanetary magnetic field by comparison of simultaneous Pioneer 10 and Heos 1, 2, data, J. Geophys. Res., 82, 1273, 1977.

Schwenn, R., M. D. Montgomery, H. Rosenbauer, H. Miggenrieder, and K. H. Mühlhäuser, S. J. Bame, W. C. Feldman, and R. T. Hansen, Direct observation of the latitudinal extent of a high-speed stream in the solar wind, J. Geophys. Res., 83, 1011, 1978.

Smith, E. J., Radial gradients in the interplanetary magnetic field between 1.0 and 4.3 AU: Pioneer 10, in Solar Wind Three, edited by C. T. Russell, University of California Press, Los Angeles, 1974.

Smith, E. J., and J. H. Wolfe, Observations of interaction regions and corotating shocks between 1 and 5 AU; Pioneers 10 and 11, Geophys. Res. Lett., 3, 137, 1976.

Smith, E. J., and J. H. Wolfe, Pioneer 10, 11 observations of evolving solar wind streams and shocks beyond 1 AU, in Study of Traveling Interplanetary Phenomena/1977, edited by M. A. Shea, D. F. Smart, and S. T. Wu, pp. 227-257, D. Reidel, Hingham, Mass., 1977.

Smith, E. J., Tsurutani, B. T., and Rosenberg, R. L. Observations of the interplanetary sector structure up to heliographic latitudes of 16°: Pioneer 11, J. Geophys. Res., 83, 717, 1978.

Smith, E. J., Interplanetary magnetic fields, Rev. Geophys. Space Phys., 17, 610, 1979.

Svalgaard, L., and J. M. Wilcox, A view of solar magnetic fields, the solar corona, and the solar wind in three dimensions, Ann. Rev. Astrophys., 16, 429, 1978.

Thomas, B. T. and E. J. Smith, The Parker spiral configuration of the interplanetary magnetic field between 1 and 8.5 AU, J. Geophys. Res., 85, 6861, 1980.

Villante, U. and F. Mariani, On the radial variation of interplanetary magnetic field: Pioneer 6, Geophys. Res. Lett., 2, 73, 1975.

Villante, U., R. Bruno, F. Mariani, L. F. Burlaga, and N. F. Ness, The shape and location of the section boundary surface in the inner solar system, J. Geophys. Res., 84, 6641, 1979.

Whang, Y. C., Alfvén waves in spiral interplanetary field, J. Geophys. Res., 78, 7221, 1973.

FIGURE CAPTIONS

FIGURE 1 — The radial variation of $\underset{\sim}{B}(R)$ in heliographic coordinates, observed by Voyager 1 between 1 AU and 5 AU. The curve $B_p = A\,(1/R^2)\,(1 + R^2)^{1/2}$ is the prediction of the spiral model for $\Omega R_1/V = 1$, and the coefficient of this curve was obtained by a least squares fit of log B_p to the measurements, log $|\underset{\sim}{B}|$. The two curves for $\lambda(R)$ are the spiral model curves.

FIGURE 2 — The radial variation of $\underset{\sim}{B}(R)$ in heliographic coordinates, observed by Voyager 2 (see the caption for Figure 1).

FIGURE 3 — The distributions of B/B_p in increments of 1 AU based on daily averages of $|\underset{\sim}{B}|$. B_p is the theoretical value from the spiral model curves shown in Figures 1 and 2.

FIGURE 4 — The distribution of hour averages of $|\underset{\sim}{B}| \equiv B$ measured by IMPs 7 and 8 at 1 AU, for the years 1976, 1977, 1978 and 1979.

FIGURE 5 — The distributions of $\lambda - \lambda_p$, in increments of 1 AU for Voyagers 1 and 2; here λ_p is the theoretical value given by the spiral model $\lambda_p(R) = -\tan^{-1}\,(R_1\Omega/V)/R)$, where V is the measured solar wind speed.

FIGURE 6 — The distributions of δ in increments of 1 AU for Voyagers 1 and 2.

FIGURE 7 — Radial variations of the 24-hr averages of the absolute values of the hour averaged $|\underset{\sim}{B}|$ and components of $\underset{\sim}{B}$ measured by Voyager 1. The dashed curves are derived from the spiral model (see the caption of Figure 1). The solid curves are linear least squares fits to log B_i vs log R, i = R, T, N and total magnitude.

FIGURE 8 Radial variations of the absolute values of the 24-hour averages of the components of $\underset{\sim}{B}_S$ measured by Voyager 1 (see the caption of Figure 7).

FIGURE 9 Radial variations of 24-hour averages of σ_c, where σ_c is the RMS of a component of $\underset{\sim}{B}_S$ measured in an hour-interval. The lines are linear least squares fits to log σ_c vs log R.

FIGURE 10 Radial variations at the 24-hour averages of σ_c/B (see Figure 10).

FIGURE 11 Radial variations of the 24-hour averages of σ_B/B, where σ_B is the RMS of the magnitude of B measured in an hour-interval and B is the average field strength for that hour. The lines are linear least squares fits to log (σ_B/B) vs log R.

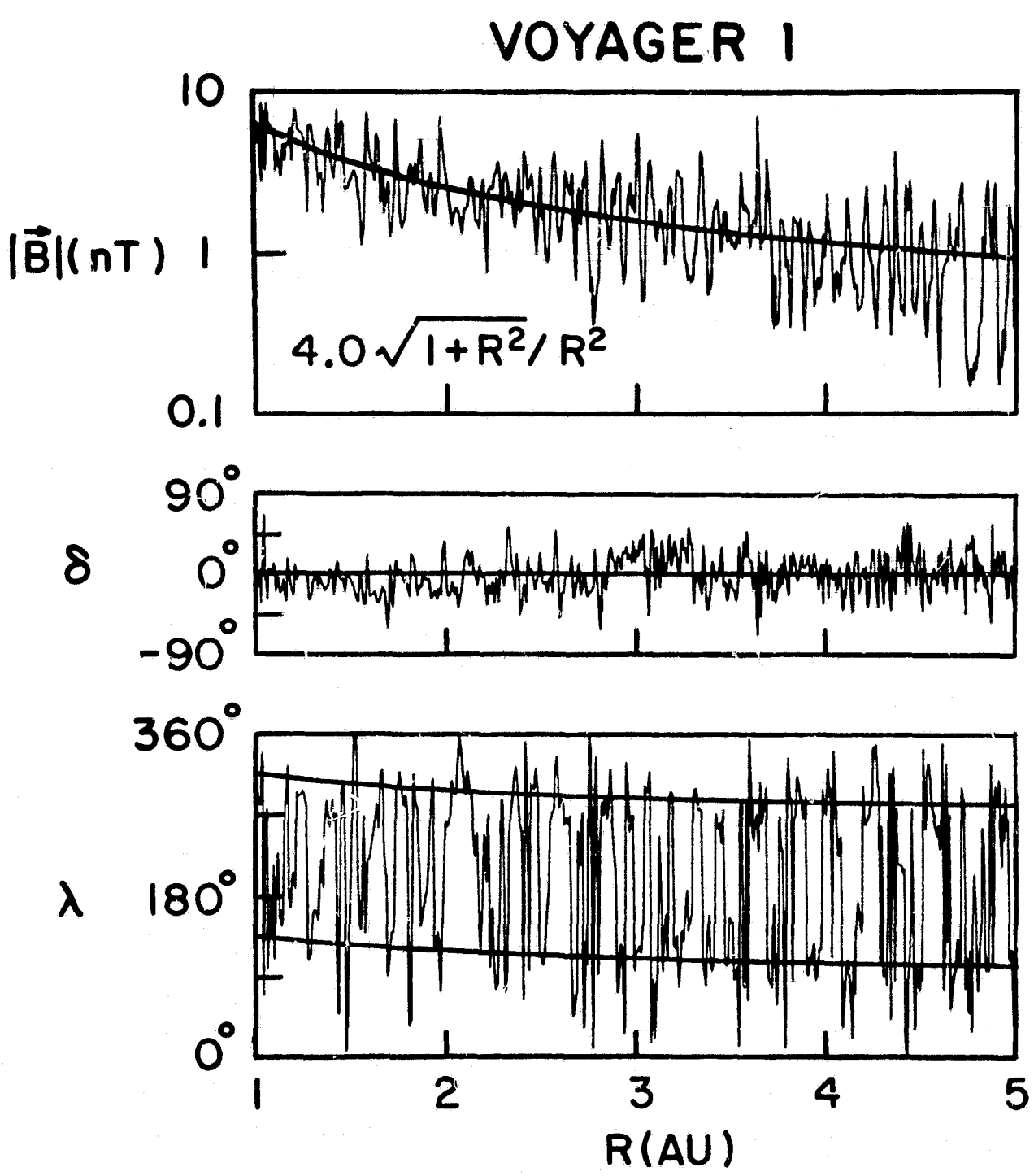

Figure 1

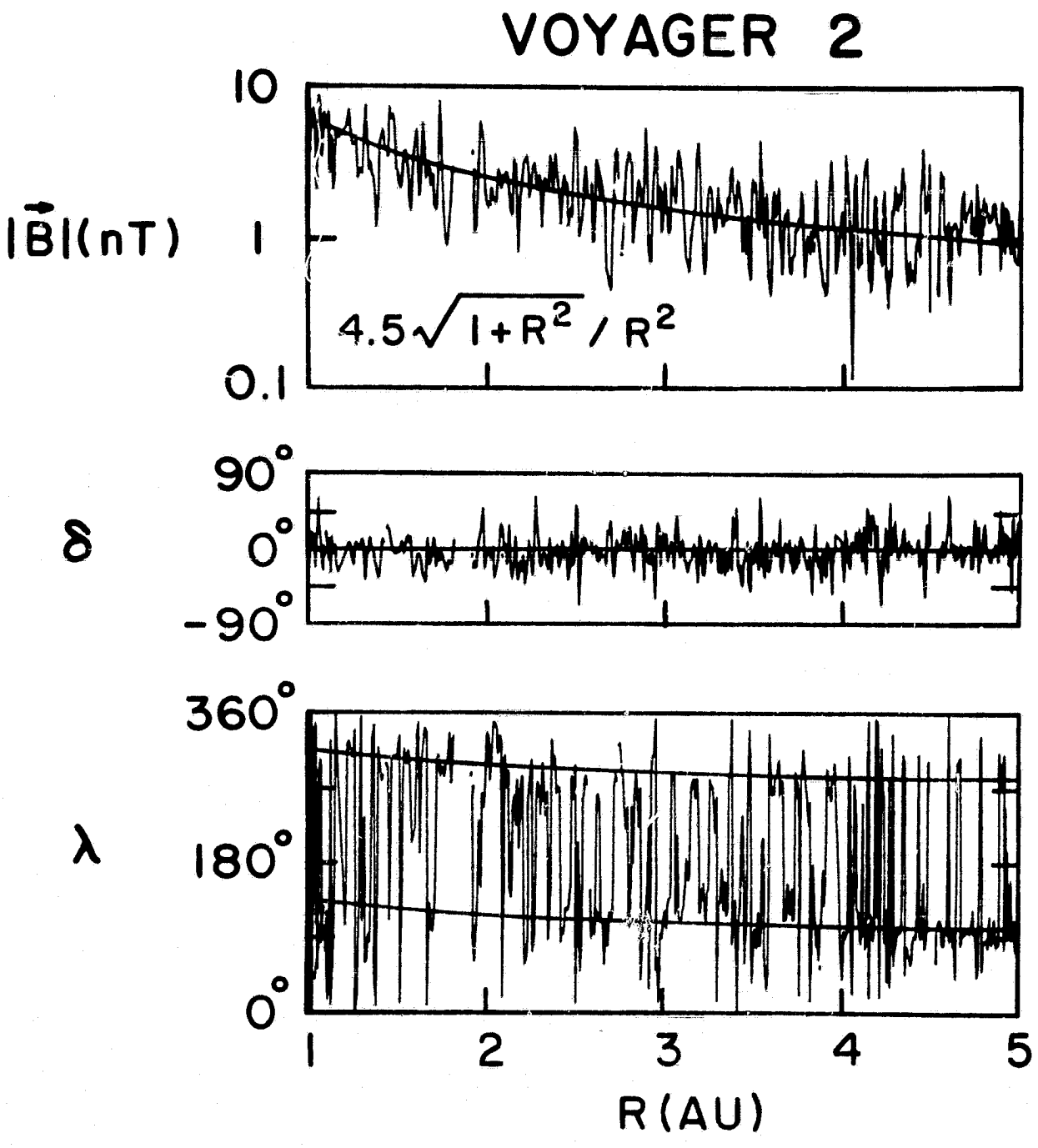
VOYAGER 2
10
1
0.1
$|\vec{B}|$(nT)
$4.5\sqrt{1+R^2}/R^2$
90°
0°
-90°
δ
360°
180°
0°
λ
1
2
3
4
5
R(AU)

Figure 2

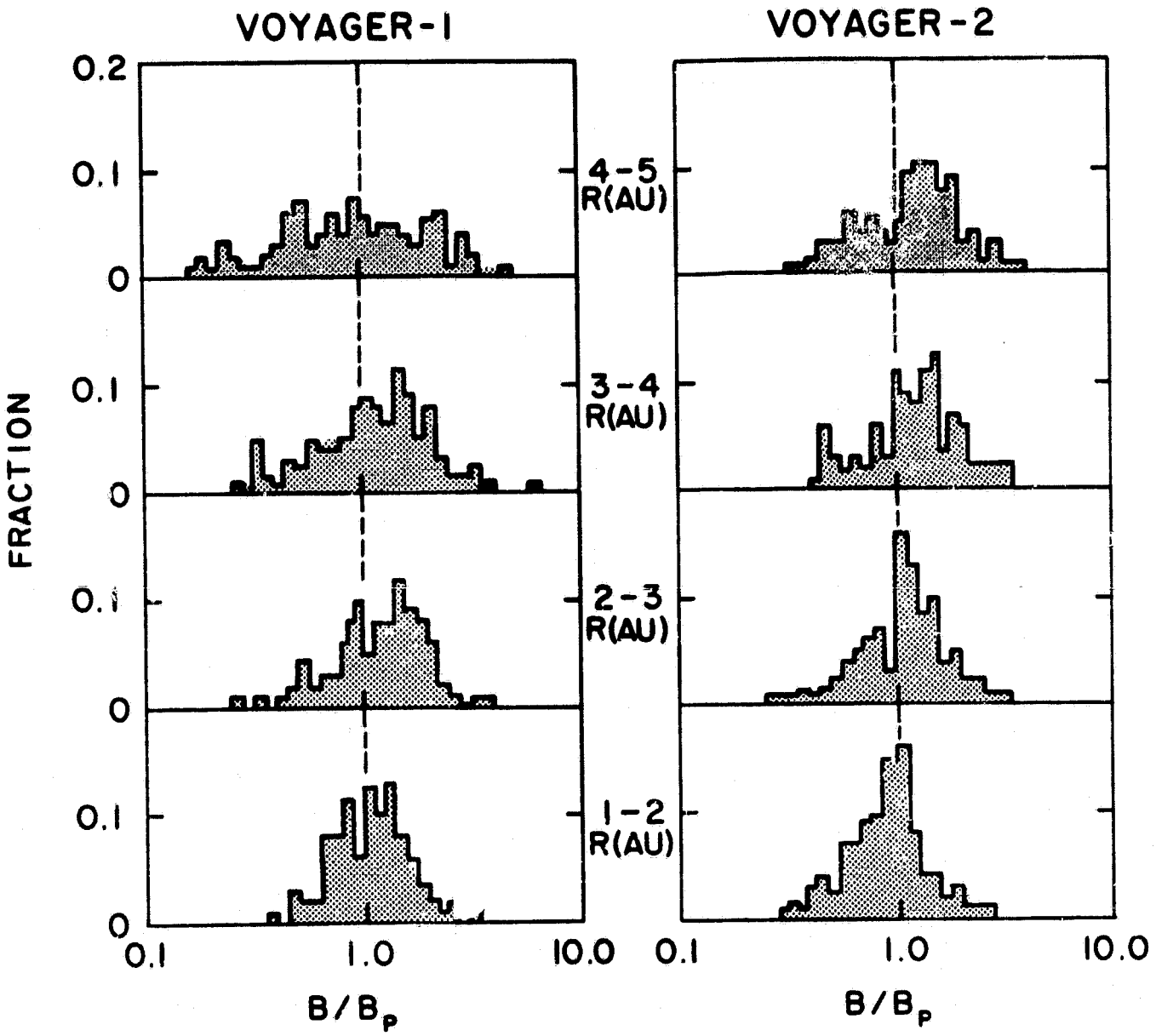
VOYAGER-1
VOYAGER-2
FRACTION
0.2
0.1
0
4-5 R(AU)
3-4 R(AU)
2-3 R(AU)
1-2 R(AU)
0.1
1.0
10.0
B/B_P

Figure 3

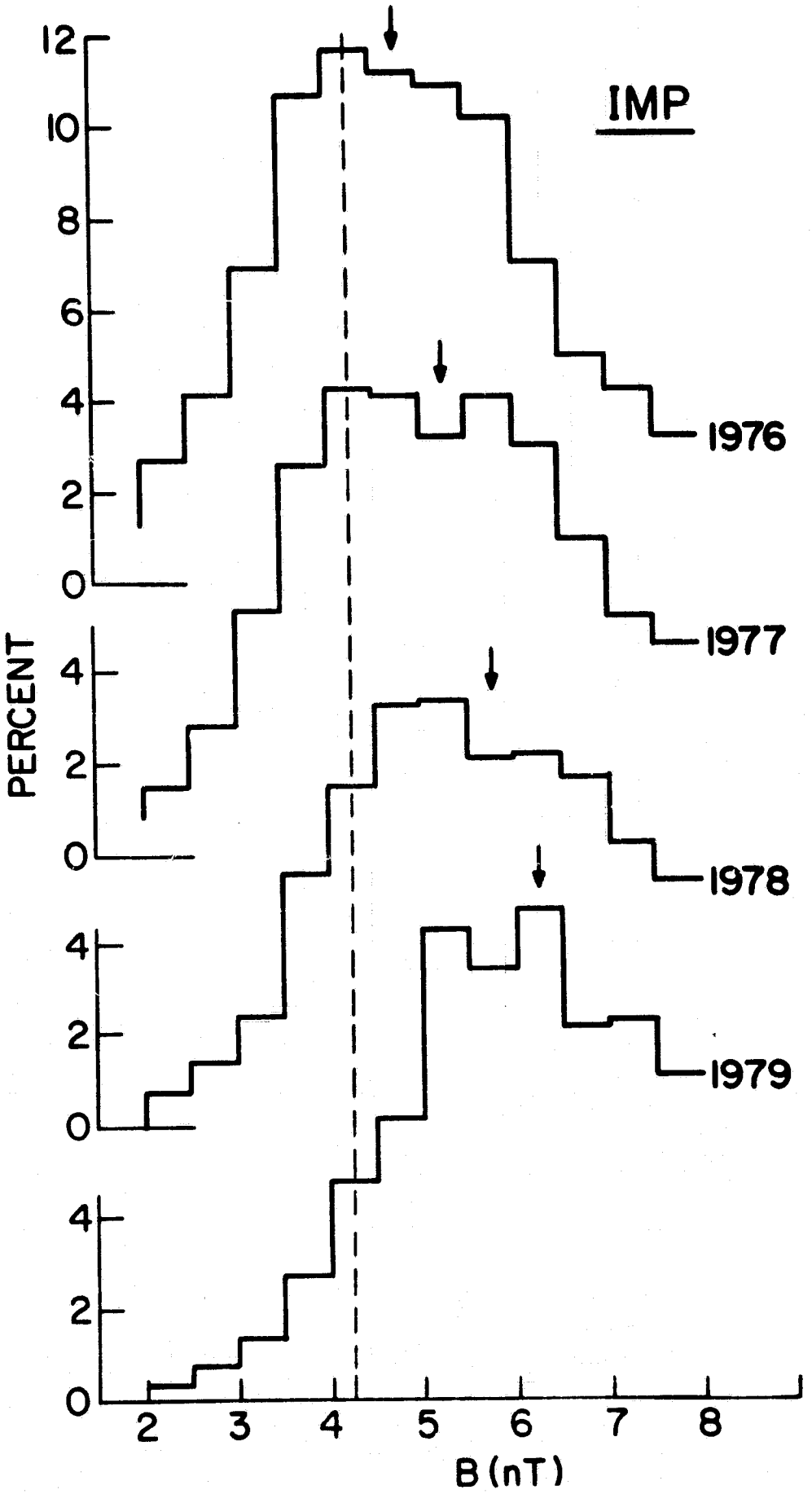

Figure 4

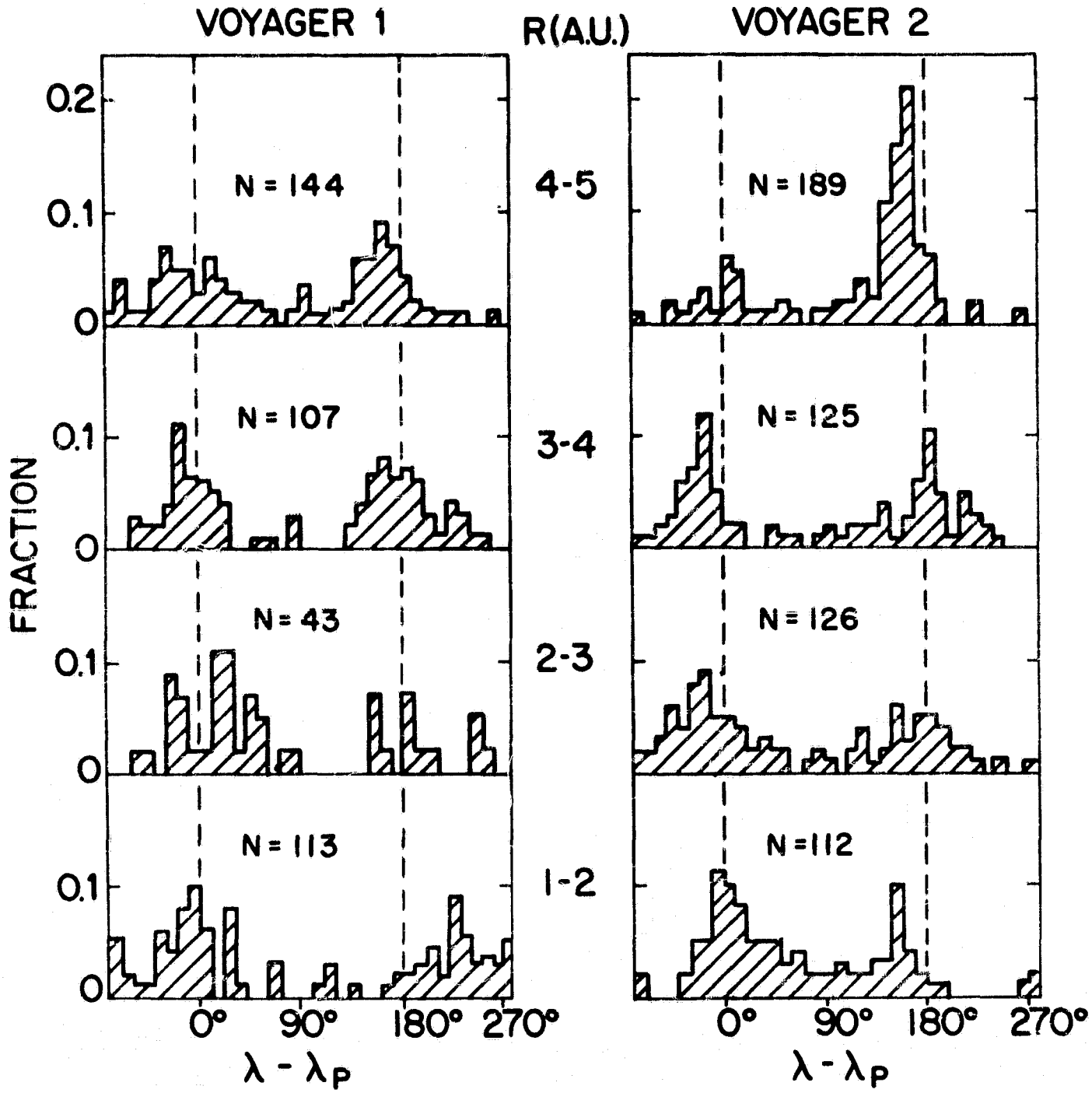
VOYAGER 1
R(A.U.)
VOYAGER 2
0.2
0.1
0
N = 144
4-5
N = 189
0.1
0
N = 107
3-4
N = 125
FRACTION
0.1
0
N = 43
2-3
N = 126
0.1
0
N = 113
1-2
N = 112
0°
90°
180°
270°
λ - λP
0°
90°
180°
270°
λ - λP

Figure 5

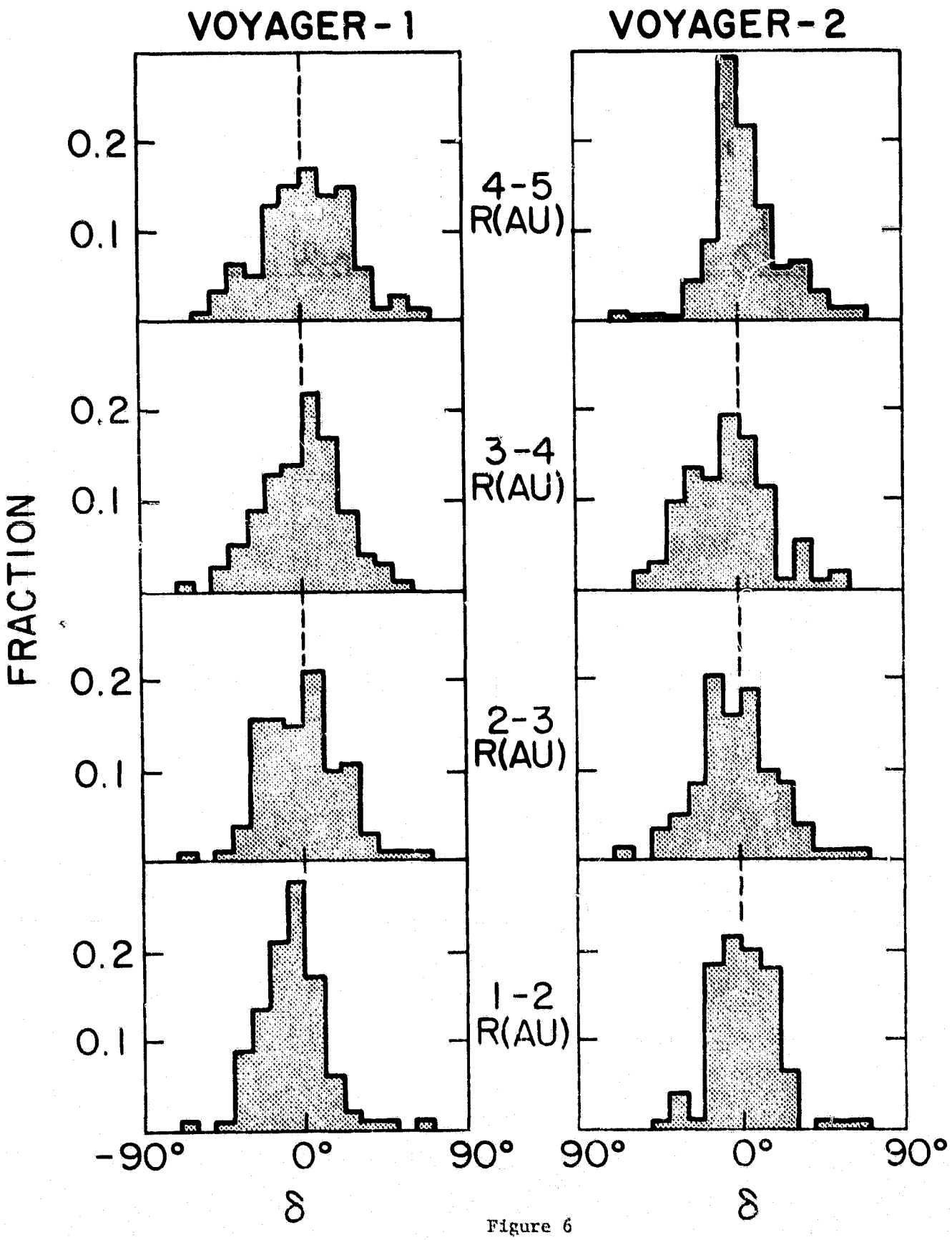
VOYAGER-1
VOYAGER-2
FRACTION
0.2
0.1
4-5 R(AU)
3-4 R(AU)
2-3 R(AU)
1-2 R(AU)
-90°
0°
90°
δ

Figure 6

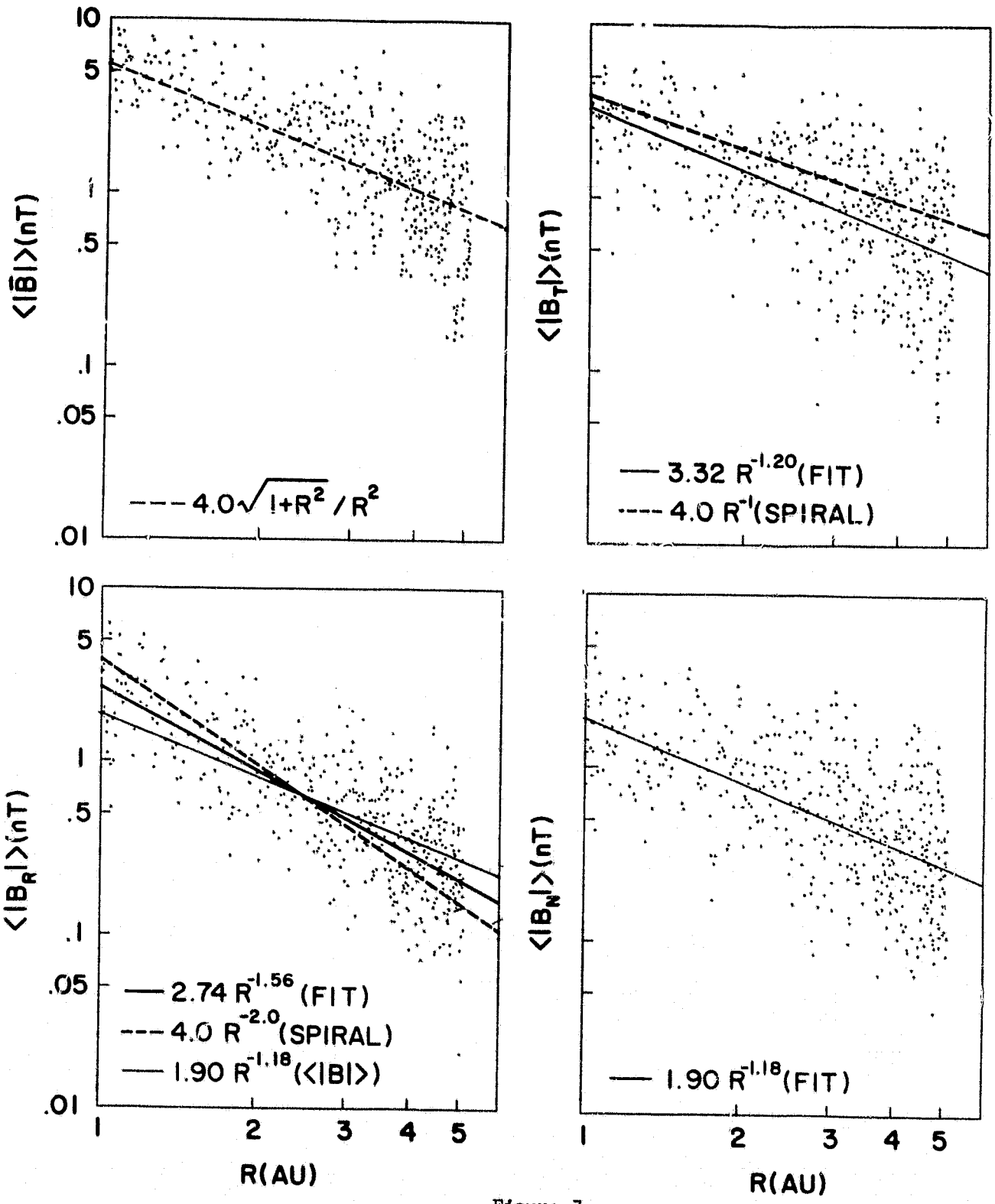
VOYAGER 1
10
5
1
.5
.1
.05
.01
<|B|>(nT)
--- 4.0√(1+R²)/R²
<|B_T|>(nT)
— 3.32 R^-1.20 (FIT)
---- 4.0 R^-1 (SPIRAL)
<|B_R|>(nT)
— 2.74 R^-1.56 (FIT)
--- 4.0 R^-2.0 (SPIRAL)
— 1.90 R^-1.18 (<|B|>)
1
2
3
4
5
R(AU)
<|B_N|>(nT)
— 1.90 R^-1.18 (FIT)
R(AU)

Figure 7

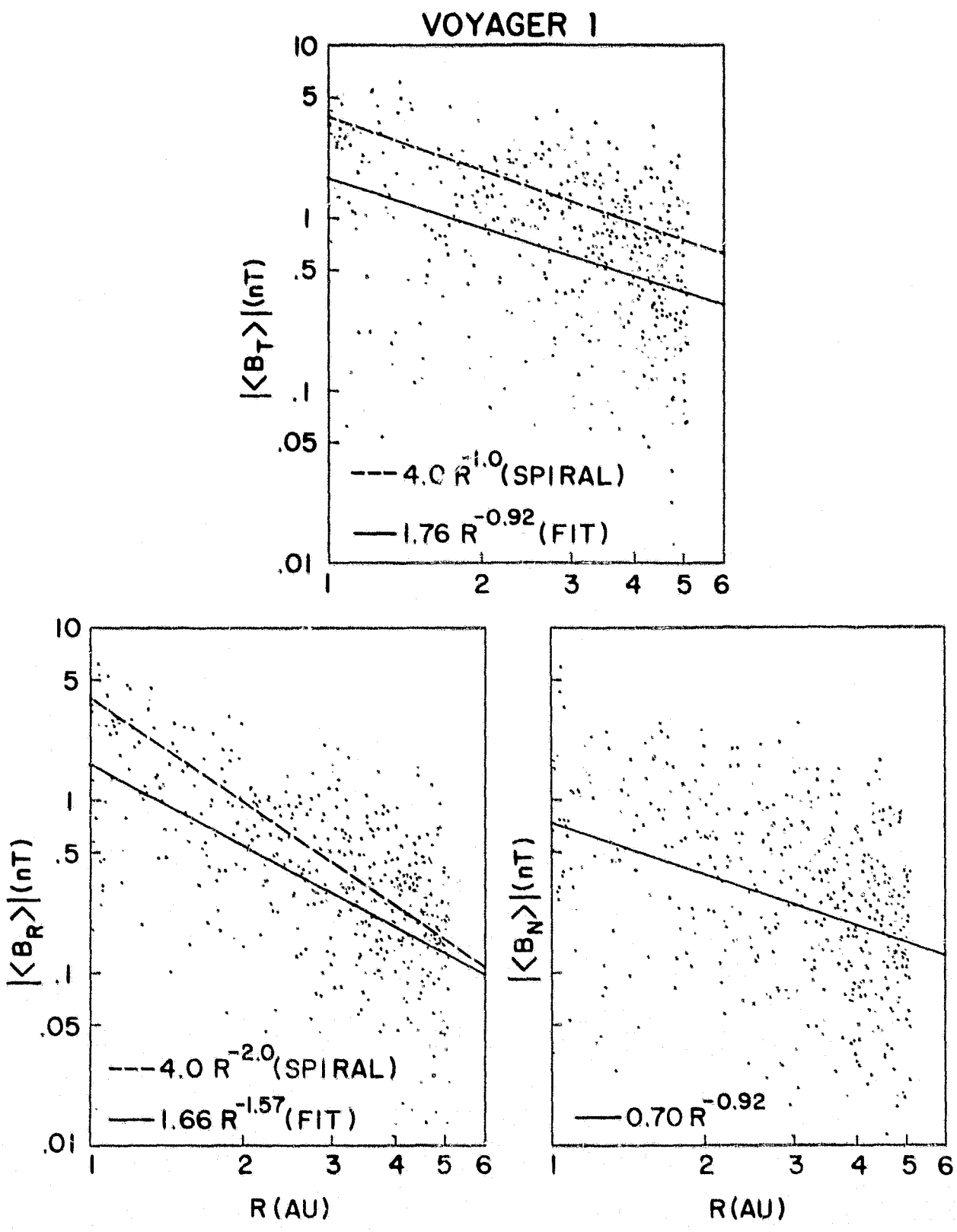
VOYAGER 1
10
5
1
.5
.1
.05
.01
$|\langle B_T \rangle|$(nT)
---4.0 $R^{-1.0}$(SPIRAL)
—1.76 $R^{-0.92}$(FIT)
1
2
3
4
5
6
$|\langle B_R \rangle|$(nT)
---4.0 $R^{-2.0}$(SPIRAL)
—1.66 $R^{-1.57}$(FIT)
R(AU)
$|\langle B_N \rangle|$(nT)
—0.70 $R^{-0.92}$
R(AU)

Figure 8

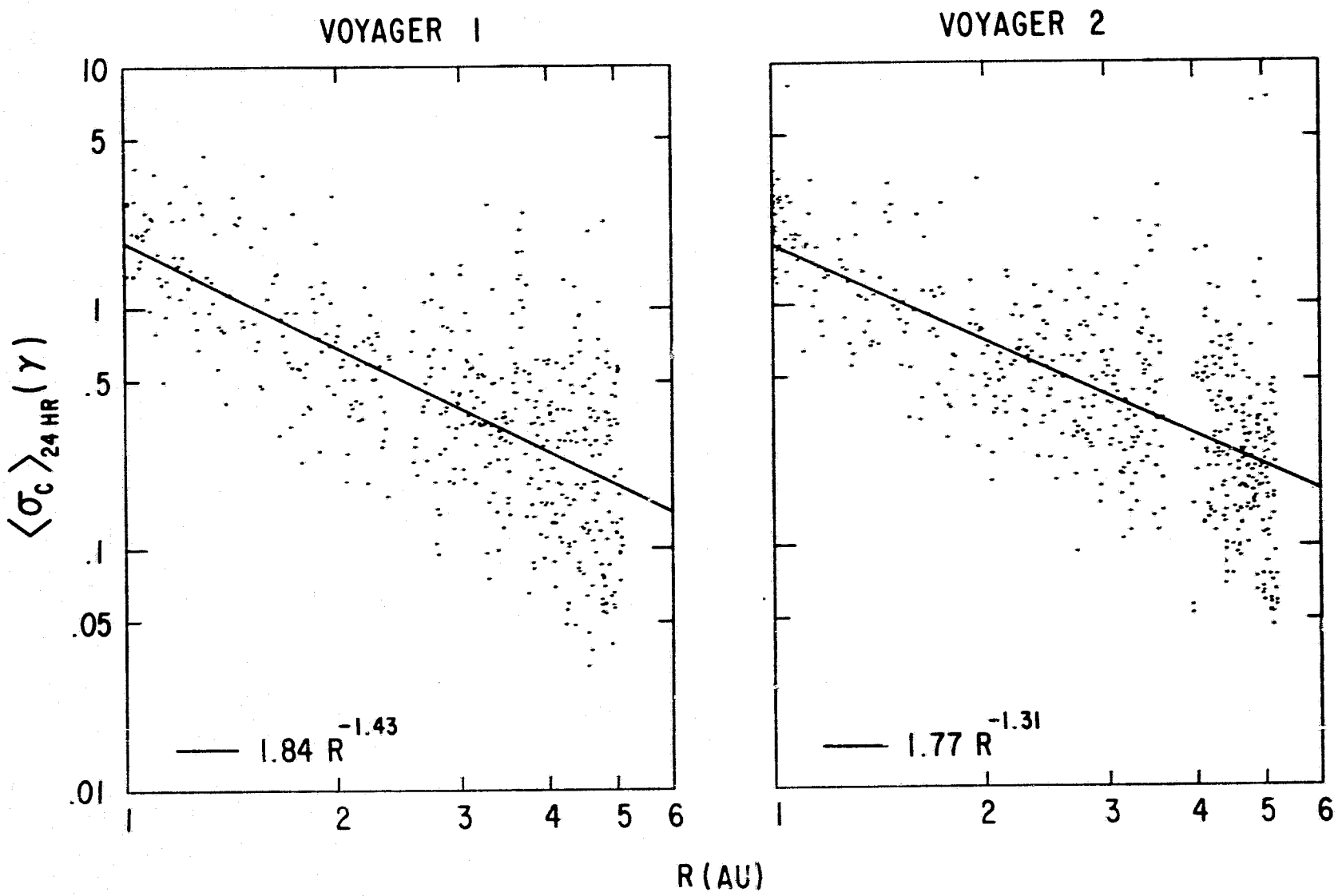
VOYAGER 1
VOYAGER 2
10
5
1
.5
.1
.05
.01
$\langle \sigma_c \rangle_{24\,HR}(\gamma)$
1.84 R^-1.43
1.77 R^-1.31
1
2
3
4
5
6
R (AU)

Figure 9

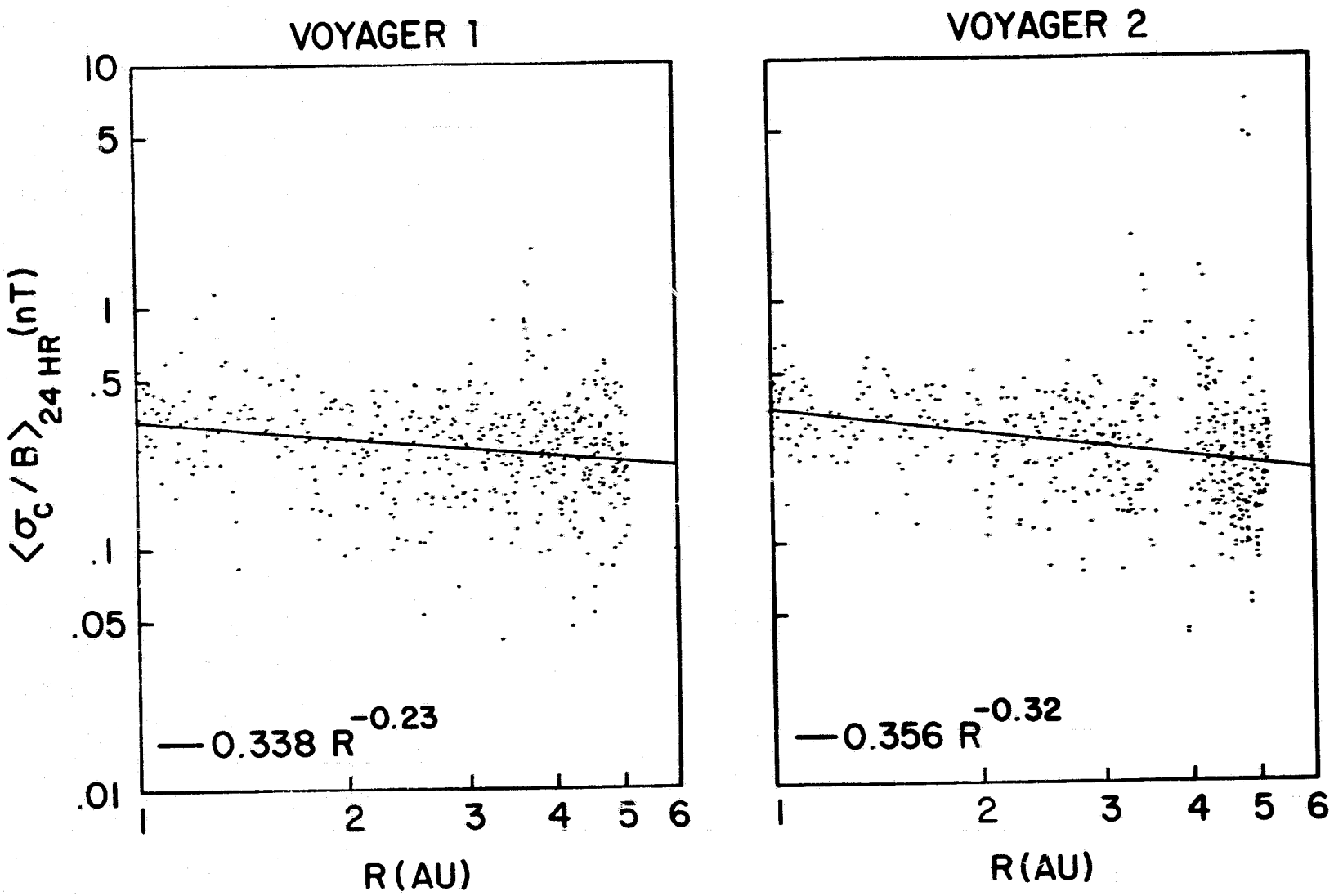
VOYAGER 1
VOYAGER 2
10
5
1
.5
.1
.05
.01
$\langle \sigma_c / B \rangle_{24\,HR}$ (nT)
— 0.338 R$^{-0.23}$
— 0.356 R$^{-0.32}$
1
2
3
4
5
6
R(AU)
R(AU)

Figure 10

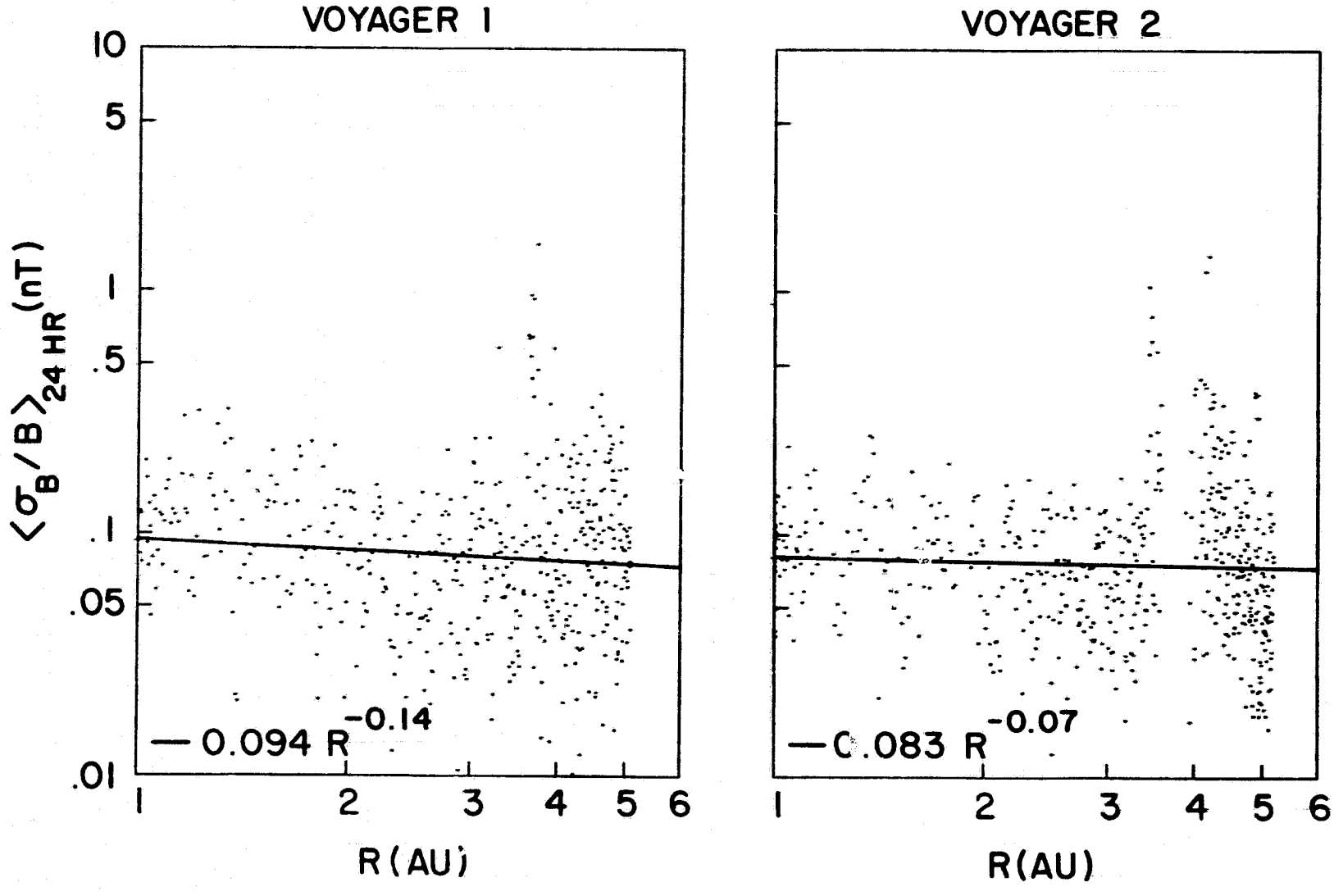
VOYAGER 1
VOYAGER 2
10
5
1
.5
.1
.05
.01
$\langle \sigma_B / B \rangle_{24\,HR}$ (nT)
— 0.094 R$^{-0.14}$
— 0.083 R$^{-0.07}$
1
2
3
4
5
6
R(AU)
R(AU)

Figure 11